

# Lithium Adsorption on Graphene: From Isolated Adatoms to Metallic Sheets

A. M. Garay-Tapia,<sup>†,§</sup> Aldo H. Romero,<sup>†</sup> and Veronica Barone<sup>\*,‡</sup>

<sup>†</sup>CINVESTAV-Unidad Querétaro, Libramiento Norponiente 2000, CP 76230, Querétaro, México

<sup>‡</sup>Department of Physics and Science of Advanced Materials Program, Central Michigan University, Mount Pleasant, Michigan 48859, United States

**ABSTRACT:** We have studied Li adsorption on graphene for Li concentrations ranging from about 1% to 50% by means of density functional theory calculations. At low adsorbant densities, we observe a strong ionic interaction characterized by a substantial charge transfer from the adatoms to the substrate. In this low concentration regime, the electronic density around the Li adatoms is well localized and does not contribute to the electronic behavior in the vicinity of the Fermi level. For larger concentrations, we observe the formation of a chemically bound Li layer characterized by a stronger binding energy as well as a significant density of states above the Fermi level coming from both graphene and the two-dimensional Li sheet.

## 1. INTRODUCTION

Experimental and computational studies of graphene and its lower-dimensional derivatives have exploded in the past few years since graphene synthesis was first reported in 2004.<sup>1</sup> The unique electronic and mechanical properties of these materials open a venue for exciting applications in a variety of technologies such as electronics, sensors, and energy storage.<sup>2–16</sup> Tunable control of the electronic properties of graphenes achieved by doping or edge chemical modification is needed in order to enhance their range of potential applications.<sup>17</sup> The adsorption of metal atoms on graphene materials presents yet another way of achieving this goal and has been recently investigated by ab initio techniques.<sup>18–24</sup> Among the metals that can be adsorbed on graphene, Li is particularly important for applications in hydrogen storage, Li-ion batteries, and superconductors.<sup>25–28</sup> It is generally accepted that the interaction between Li atoms and graphene presents an ionic character with a substantial charge transfer from the adsorbate to the carbon substrate.<sup>29–32</sup>

Most of the calculations carried on in these types of systems are performed utilizing density functional theory (DFT) which might fictitiously favor ionic interactions over weaker dispersive interactions. However, a recent study utilizing an approach beyond DFT has demonstrated that the ionic bonding of Li on graphenes is actually the main interaction mechanism, thus validating DFT calculations in these kinds of systems.<sup>33</sup> Few works discuss the interaction of Li and graphene at various Li concentrations.<sup>22,34–36</sup> Here, we concentrate on the systematic study on the effect of Li concentration on the geometrical and electronic properties of  $\text{Li}_x\text{C}$  systems with  $x$  varying from about 0.01 to 1.

## 2. METHODOLOGY

Calculations have been performed using DFT as implemented in the Vienna *ab-initio* simulation package (VASP)<sup>37,38</sup> employing the GGA-PBE functional.<sup>39</sup> Wave functions are expanded in plane waves, using only valence electrons described within

the projector augmented-wave (PAW)<sup>40</sup> pseudopotentials formalism.

In order to study the adatom concentration effects on the energetics of the systems, we have utilized several different supercells that allow Li concentrations to vary from 1% to 50%. We chose a  $2 \times 2 \times 1$  supercell with a k-point mesh of  $21 \times 21 \times 1$  and cutoff energy of 550 eV for concentrations higher than 10% and  $3 \times 3 \times 1$ ,  $4 \times 4 \times 1$ ,  $6 \times 8 \times 1$ , and  $6 \times 6 \times 1$  supercell models with k-point meshes of  $8 \times 8 \times 1$ ,  $6 \times 6 \times 1$ ,  $6 \times 9 \times 1$ , and  $3 \times 3 \times 1$ , respectively, for concentration ranging from 1% to 10%. To avoid interactions between images along the Z axis (perpendicular to the graphene plane), a Z-size box of 20 Å has been considered.

All of the structures have been fully relaxed to account for any rearrangement in the graphitic surfaces due to the presence of the Li atoms until the maximum and root-mean-square atomic forces are less than 0.008 eV/Å.

It is well established that, in the case of low Li concentrations, the most stable adsorption site corresponds to the hollow site (on top of the center of the hexagon) while adsorptions on top of the C atom and in the middle of the C–C bond present higher energies.<sup>41</sup> However, as the Li concentrations increase, on top of the C atom sites need to be occupied in order to obtain higher Li densities.

## 3. RESULTS AND DISCUSSION

**3.0.1. Low Li Concentrations.** We will first discuss our results for the optimal Li-graphene plane distance for different configurations of Li adsorbed on graphene at low Li concentrations (from 1% to 10%). The results presented in Table 1 correspond to several models that are identified with the labels A–B, where A corresponds to the number of C atoms in the supercell and B, the number of Li atoms. The molar fraction of Li is then obtained for each system as  $X = B/(A + B)$ . For the case of the Li atom adsorbed on top of the center of the

Received: January 23, 2012

Published: February 15, 2012



**Table 1.** Binding Distances: Average Value Perpendicular to the Carbon Ring, ( $d_{\perp\text{ring}}$ ) and Average Value Perpendicular to the Carbon Atoms, ( $d_{\perp\text{C}}$ )

model	$d_{\perp\text{ring}}(\text{\AA})$	$d_{\perp\text{C}}(\text{\AA})$	composition $x(\text{Li})$
18-2		2.019	0.1000
18-2c	1.675	2.207	0.1000
18-1		2.022	0.0526
18-1c	1.651	2.191	0.0526
32-1		1.987	0.0303
32-1c	1.689	2.218	0.0303
48-1		2.003	0.0204
48-1c	1.700	2.226	0.0204
72-1		2.012	0.0136
72-1c	1.713	2.237	0.0136

hexagon, we use the label A–Bc. The model 32–1c corresponds to a  $4 \times 4$  graphene supercell. The distance of about 1.69 Å from the Li atom to the graphene plane for this model is in good agreement with previous calculations at the same level of theory.<sup>42</sup>

In all cases, we note that the Li distance to the graphene plane is shorter when the Li is adsorbed on top of the hexagon, in agreement with previous results. In Table 2, we show the

**Table 2.** Average Charge Calculated Using Voronoi Analysis and Maximum Charge Difference from the Average

model	C	max diff	Li	max diff
18-2	-0.040	0.076	0.357	0.016
18-2c	-0.040	-0.082	0.329	0.001
18-1	-0.021	0.07	0.395	0.000
18-1c	-0.020	0.084	0.396	0.000
32-1	-0.020	-0.073	0.529	0.000
32-1c	-0.010	-0.081	0.424	0.000
48-1	-0.010	0.075	0.551	0.000
48-1c	-0.010	-0.086	0.434	0.000
72-1	-0.010	-0.073	0.541	0.000
72-1c	-0.010	-0.086	0.445	0.000

average charge on the C and Li atoms calculated using the Voronoi analysis.<sup>43</sup> The charge transfer is largest for lowest concentrations. At the same concentrations, the average charge on the Li atom is slightly larger when the Li is adsorbed on top of the C atom than at the center of the hexagon.

In Figure 1, we present the binding energies,  $E_b$ , of Li on graphene for concentrations ranging from 1.3% to 10% when Li is adsorbed at the center of the hexagon and on top of the C atom. Several papers appeared in the literature presenting DFT calculations in  $(4 \times 4)$  graphene, which corresponds to our 32–1c model. Valencia et al.<sup>19</sup> report the Li binding energy in this system to be 1.55 eV with LSDA and 1.01 eV with the generalized gradient approximation functional of Perdew–Burke–Ernzerhof, PBE, while Chan et al. report a slightly higher binding energy of 1.10 eV with PBE.<sup>20</sup> For this model system, we obtain a binding energy of 1.29 eV (PBE), in good agreement with previous results.

Figure 1 shows the established trend of a stronger binding for the adsorption taking place at the center of the hexagon (more negative  $E_b$ ). It is found, as expected, that  $E_b$  increases for larger Li concentrations. This trend can be explained not only through the increase in the Coulomb repulsion between Li ions due to closer proximity but also through the strain caused

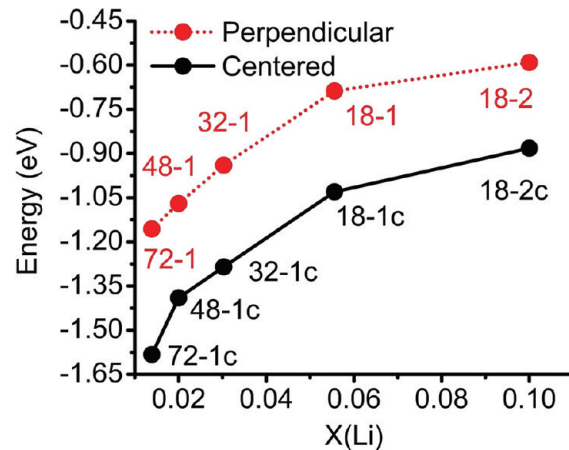


**Figure 1.** Binding energies (eV) for Li concentrations ranging from 0.13% to 10% for the perpendicular and centered configurations. Lower binding energies (more negative values) indicate more stable configurations.

**Table 3.** Li Binding Distances: Average Distance to the Graphene Plane for the on Top of the Ring Configuration ( $d_{\perp\text{ring}}$ ) and Average Distance for on Top of the C Atom Configuration ( $d_{\perp\text{C}}$ )

model	$d_{\perp\text{ring}}(\text{\AA})$	$d_{\perp\text{C}}(\text{\AA})$	composition $X(\text{Li})$
8-1		2.142	0.1111
8-1c	1.779	2.290	0.1111
8-2		2.080	0.2000
8-2c	1.768	2.284	0.2000
8-3	1.854	2.055	0.2727
8-3c	1.771	2.095	0.2727
8-4	1.930	2.086	0.3333
8-5	1.897	2.126	0.3846
8-6	2.084	2.173	0.4285
8-7		2.010	0.4666
8-8		2.008	0.5000

in the electronic states of the graphene substrate that now needs to accommodate a larger amount of negative charge as shown in Table 2.

**3.0.2. High Li Concentrations.** In Figures 2 and 3, we show the optimized structures for Li concentrations between 10% and 50%. The structures in Figure 2 still allow Li atoms to be placed either at the center of the hexagon or on top of the C atom. This is not possible for a Li concentration larger than 33% (Figure 3) where both types of sites need to be occupied in order to accommodate the adsorbants. Finally, for concentrations of 46% and 50% (models 8–7 and 8–8), the only occupied sites are those corresponding to the on top of the C atom positions. From model 8–2 on, both faces of graphene are allowed to adsorb Li atoms. This situation would be realized experimentally either by adsorption on suspended graphene<sup>44,45</sup> or on vertically aligned graphene sheets.<sup>46</sup>

In the high Li density regime, the structures relax to the minimum energy position by displacing the extra adsorbant out of the plane, as seen in Figure 2 for model 8–5. For larger Li concentrations, we find that a hexagonal arrangement of adsorbants is favored in both faces of the graphene substrate. Notably, close to the saturation regime, we find that C atoms are displaced out of the graphene plane, in agreement with recent DFT results.<sup>47</sup> In Table 3, we show the Li–graphene

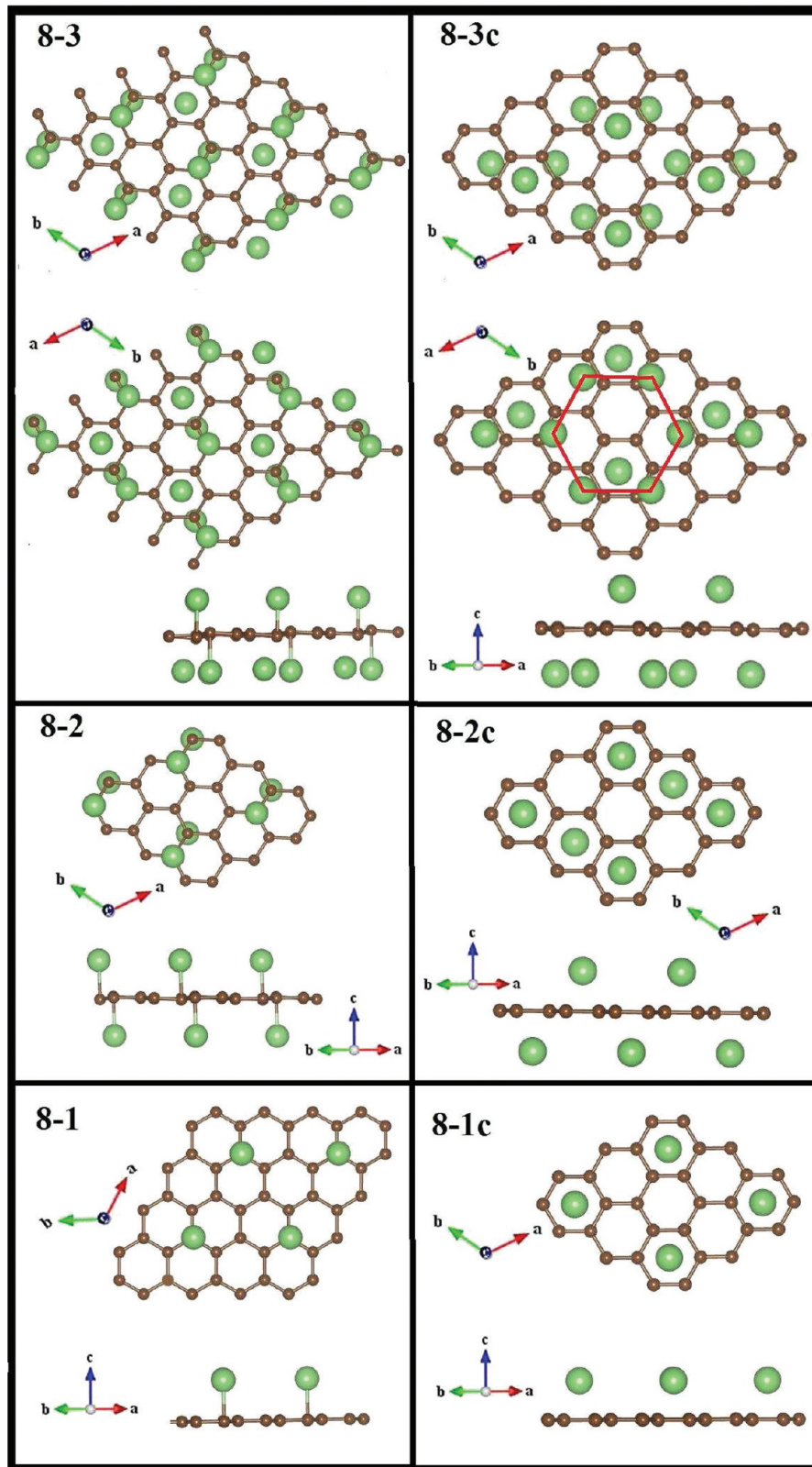


**Figure 2.** Optimized structures for Li concentrations between 10% and 27% in the perpendicular and centered positions.

plane distances for high Li densities as the Li concentration increases from about 10% to 50%, where we can appreciate that the distance between the C atom and Li in the top position decreases as the lithium concentration increases (see 8–1, 8–2, 8–3 and 8–4, 8–7, 8–8).

In Table 4, we show the average charge on the Li and C atoms as well the maximum deviation from the average obtained using the Voronoi analysis.<sup>43</sup> While in Tables 2 and 4 we observe a clear trend for Li atoms to decrease the charge transfer to the C substrate as Li concentrations

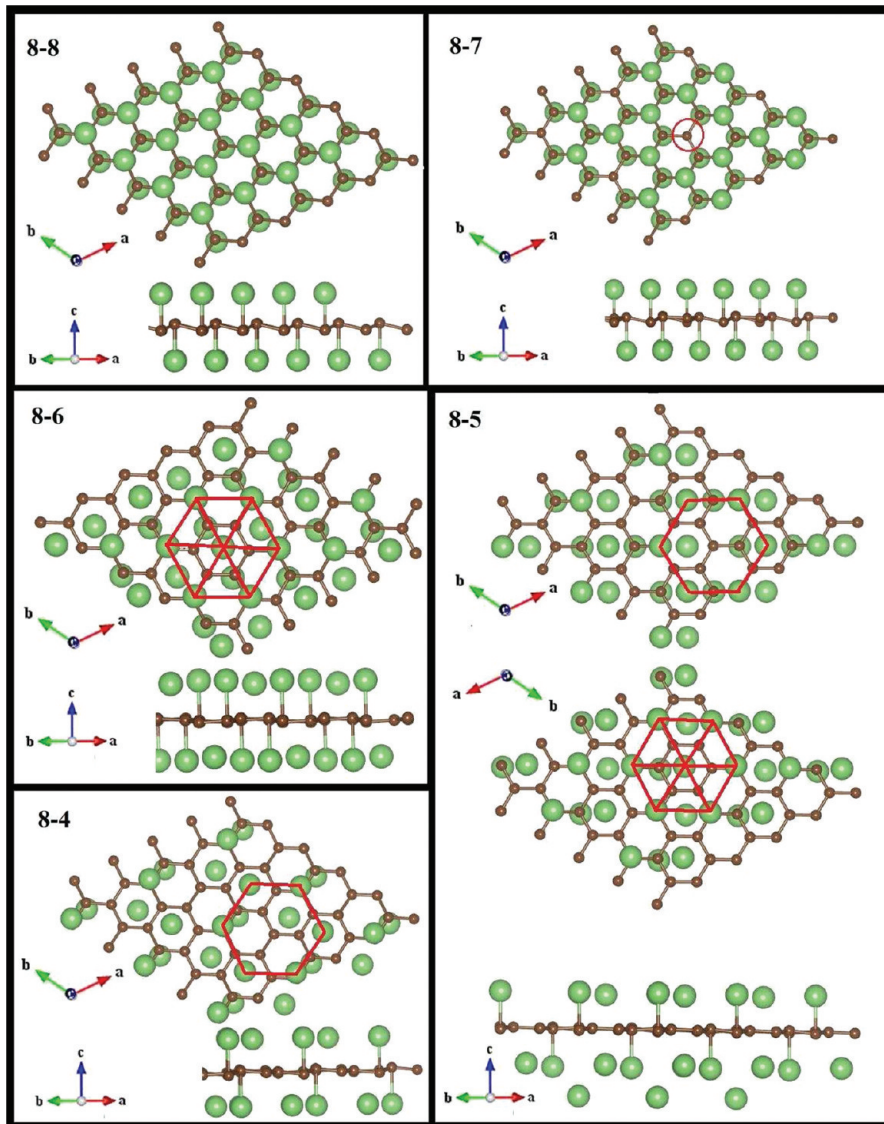


**Figure 3.** Optimized structures for Li concentrations between 33% and 50% in the perpendicular and centered positions.

**Table 4. Average Charge Calculated Using Voronoi Analysis and Maximum Charge Difference from the Average**

model	C	max diff	Li	max diff
8-1	-0.030	0.074	0.215	0.000
8-1c	-0.020	0.073	0.184	0.000
8-2	-0.050	0.029	0.219	0.002
8-2c	-0.050	-0.067	0.195	0.000
8-3	-0.050	-0.046	0.140	-0.090
8-3c	-0.050	-0.038	0.131	-0.080
8-4	-0.040	-0.028	0.090	0.008
8-5	-0.040	-0.028	0.067	0.096
8-6	-0.040	-0.014	0.060	0.030
8-7	-0.010	0.042	0.016	0.031
8-8	-0.010	-0.013	0.020	0.010

increase, the amount of charge per C atom received by the graphene substrate behaves differently. The average charge per C atom increases up to Li concentrations of about 30%, and for concentrations close to saturation, the average charge on the substrate is as small as in the low density regime.

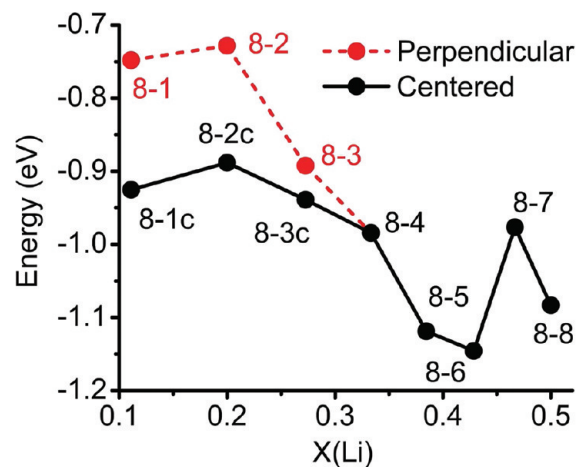


**Figure 4.** Binding energies (eV) for Li concentrations ranging from 10% to 50% for the perpendicular and centered configurations. Lower binding energies (more negative values) indicate more stable configurations.

In Figure 4, we show the Li binding energies per adsorbant for Li concentrations ranging from 10% to 50%. The figure

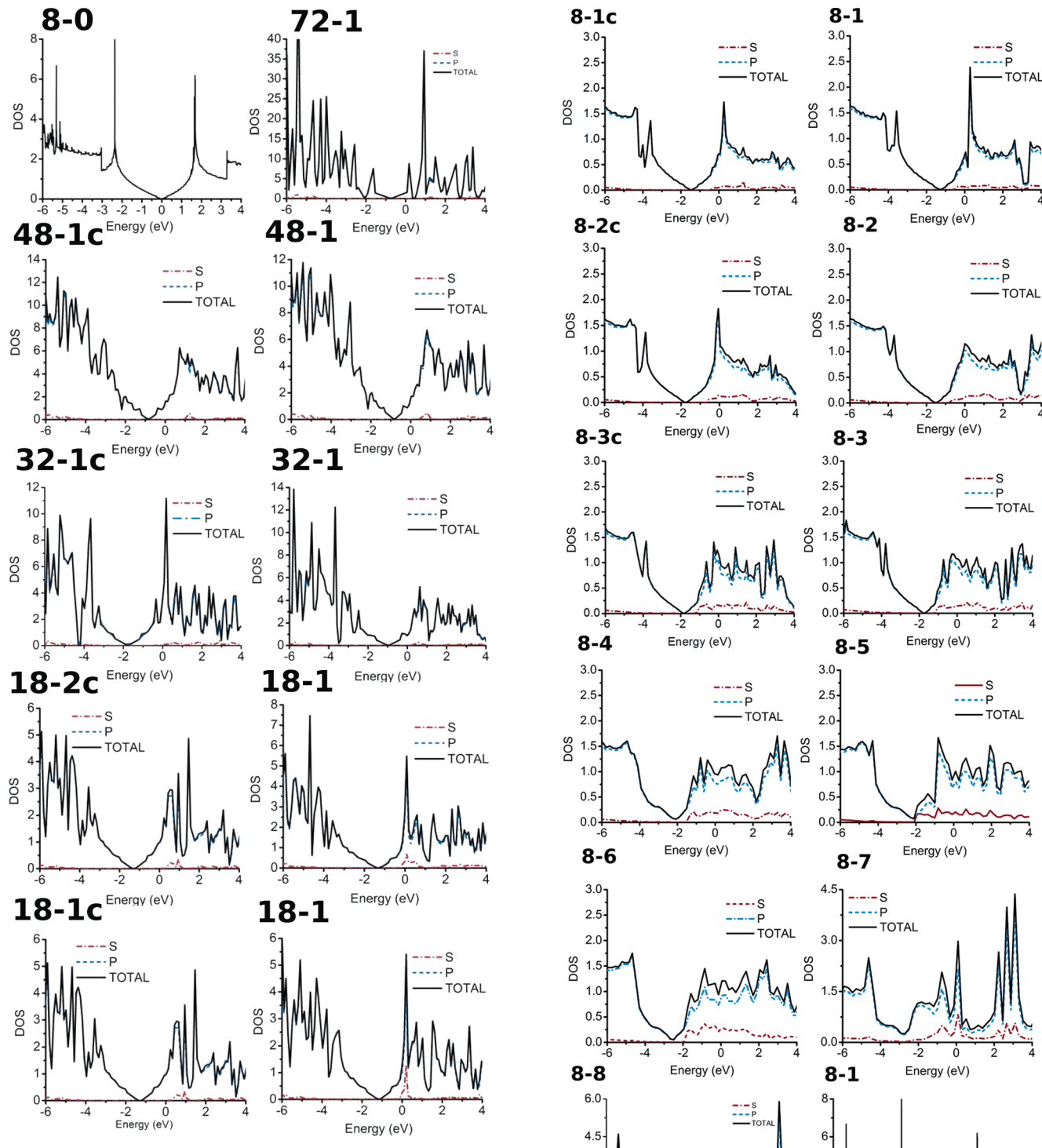


**Figure 5.** Density of states for Li-graphene systems at low Li densities. The Fermi level is set at zero.

shows that  $E_b$  increases up to Li concentrations of 20% (model 8–2) and then decreases up to a minimum that occurs for the structure 8–6. This  $E_b$  is almost as low as for the 72–1 model, indicating the presence of another interaction mechanism. This mechanism seems to correspond to the formation of Li metal on both surfaces of graphene, consistent with the systematic Li charge transfer decrease shown in Table 4.

**3.0.3. Density of States.** To examine the effect of the adsorbants on the electronic properties of these systems, we show in Figures 5 and 6 the total and partial density of states

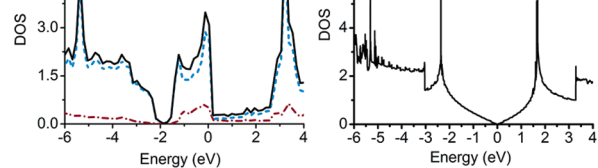


**Figure 6.** Density of states for Li-graphene systems at high Li densities. The Fermi level is set at zero.

(DOS) for the low and high Li densities, respectively. In both figures, we include the density of states of pristine graphene in a  $2 \times 2 \times 1$  cell for comparison purposes. In the low Li concentration regime (Figure 5), we see that all features around

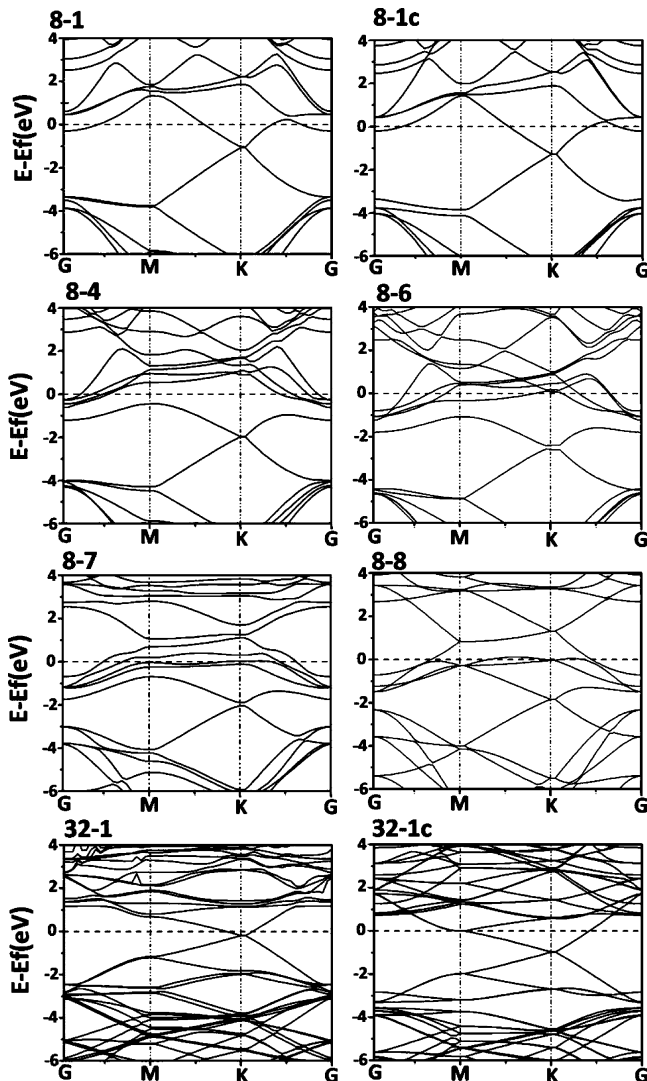


Figure 7. The band structure of some selected Li–graphene models.

the Fermi level are dominated, as expected, by the p orbital contributions from the C atoms. The charge transfer from the Li atom to the substrate produces mostly a shift in the Fermi level that turns all of these structures into metals.

For concentrations larger than 30%, the s orbital contributions to the DOS become significant. This might also be indicative of a transition from individual adsorbants to a metallic Li layer at high densities<sup>34</sup> and will be discussed further in the next section.

The band structure for some selected models are shown in Figure 7. It is observed that the number of partially occupied bands increases as the Li concentration increase. Some of these bands correspond to Li states, as shown in the partial DOS of Figure 8, where we observe that the Li contribution to the DOS around the Fermi level becomes more important as the Li density increases.

In Figure 9, we show the electron density for different Li concentrations. At low Li concentrations, the electrons are either well localized at the adsorbant or delocalized in the  $\pi$  orbitals of graphene. In model 8-1, the electrons at the Li atoms start delocalizing toward the neighboring Li, favoring the Li metal layer. For higher concentrations, we observe the

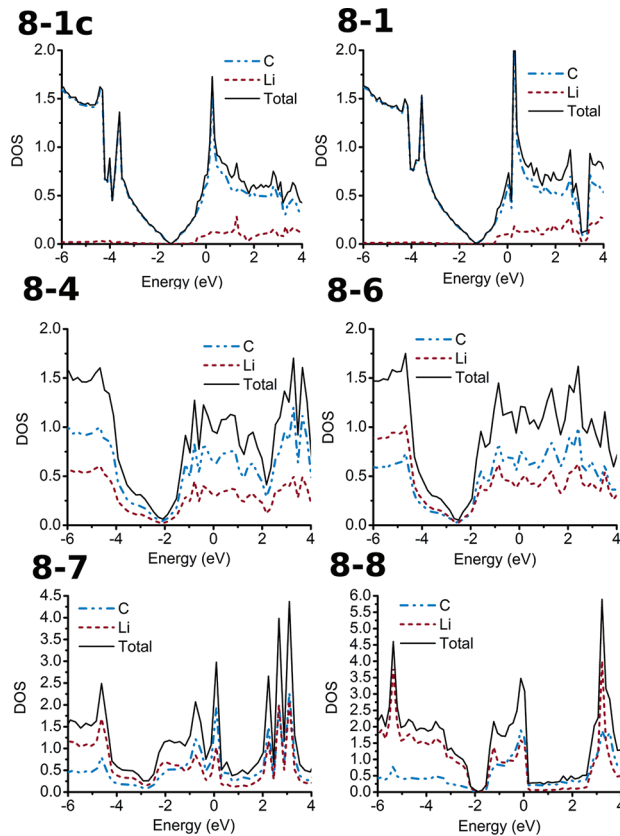
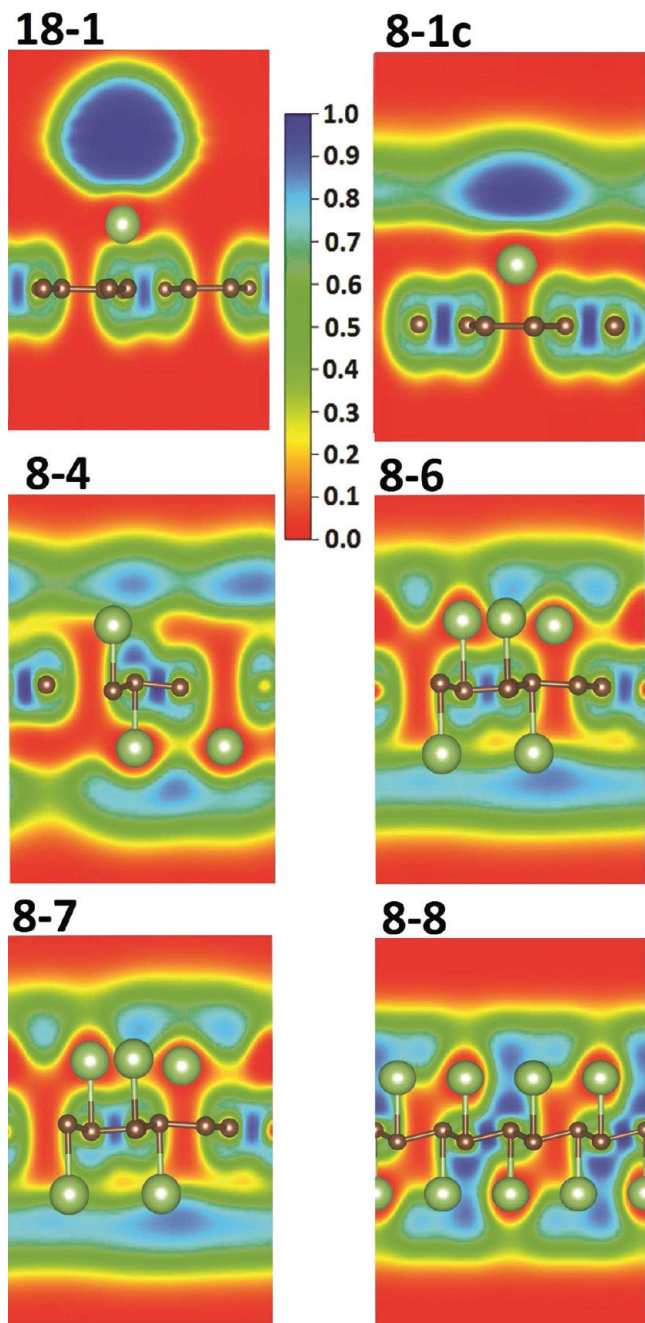


Figure 8. Density of states and partial density from Li and C orbitals for some selected models. The Fermi level is set at zero.

electronic density connecting both Li–Li and Li–C atoms, indicating a covalent bond character.

#### 3.0.4. From a Single Adsorbant to a Metallic Sheet.

For high Li concentrations, the Li binding energy decreases significantly (models 8-4 to 8-8). This stronger binding is attributed to the formation of a Li metal sheet that strongly interacts with the carbon substrate as the Li density increases. This interaction produces an atomic arrangement within graphene in which C atoms are displaced out of the plane. In order to understand this mechanism, we performed calculations on the isolated C substrate (with the modified geometry) and the isolated Li configuration and compared these structures with the combined high Li density Li–C systems. Our results are shown in Figure 10, where the DOS for each of the components normalized to the number of electrons per unit cell is plotted. For low density of adsorbants, the metallic character of the combined system arises solely from the charge transfer mechanism, which is suppressed when we consider the Li adsorbants and the graphene sheet separately. For higher Li concentrations (8-4 and higher), we start observing a significant contribution to the DOS around the Fermi level of the isolated metallic Li sheet, indicating that the metallic character of the combined systems arises in these cases from both the Li sheet and the charge transfer mechanism. A measure of the strength of the interaction between the metallic Li layer and the C substrate can be estimated by calculating it as the energy difference between the total Li–C system on one hand and the Li sheet and carbon substrate on the other, each of them at a fixed geometry. These energies are presented in Figure 10. As expected, for the low density regime, this interaction energy gives exactly the binding energy of the



**Figure 9.** Electron density plots for different Li concentrations.

system as it corresponds to the situation of having the graphene sheet plus the isolated adatom. As the concentration of Li increases, the binding energy decreases as discussed earlier. From concentrations corresponding to model 8–1 up to model 8–6, we observe that while the binding energy of the whole system decreases as shown in Figure 4, the interaction between Li and C (shown in the lower panel of Figure 10) actually keeps weakening. This effect can be explained by the formation of a bound Li sheet. Therefore, in this regime, Li and C barely interact with each other, but rather Li forms a metallic sheet, thus decreasing the binding energy of the combined system. This picture is also consistent with the systematic decrease in the Li charge of models 8–1 and up shown in Table 4. At a concentration corresponding to model 8–6, this trend is reversed, and the metallic Li sheet starts interacting with the C

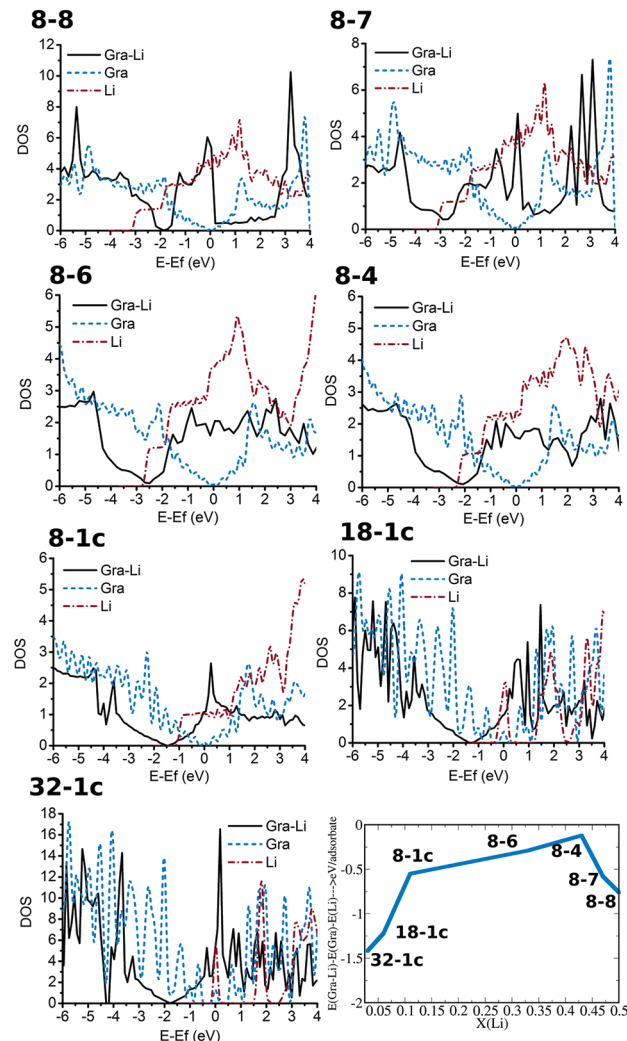


**Figure 10.** Density of states and interaction energies for the Li–C system, isolated Li in the Li–C configuration, and isolated C in the Li–C configuration for various Li concentrations. All energies in eV.

substrate in a more pronounced manner. However, due to the negligible charge transfer from C to Li observed in Table 4, we can infer that the interaction mechanism is covalent in nature at high Li concentrations. This trend is in line with the electron density plots of Figure 9.

#### 4. CONCLUSIONS

We have studied Li adsorption on graphene for Li concentrations ranging from about 0.01% to 50% by means of density functional theory calculations. At low adsorbant densities, we observe a strong ionic interaction characterized by a substantial charge transfer from the adatoms to the substrate. In this low concentration regime, the electronic density around the Li adatoms is well localized and does not contribute to the electronic behavior in the vicinity of the Fermi level. For larger concentrations, we observe the formation of a chemically bound Li layer characterized by a decrease in the binding energy as well as a significant density of unoccupied states coming from both graphene and the two-dimensional Li sheet.

By isolating the interactions due to Li–C and Li–Li, we were able to distinguish between two factors affecting the energetics of the entire system: Li metal sheet formation and Li–C bonding. From concentrations corresponding to model 8–1

(about 10%) up to model 8–6 (43%), we observe that while the binding energy of the whole system decreases as shown in Figure 4, the interaction between Li and C keeps weakening. This effect is explained by the formation of a bound Li sheet that stabilizes the energy of the whole system. For even larger Li concentrations, the metallic Li layer covalently bonds with the C substrate, producing a noticeable deviation of the C atoms from the planar symmetry.

## AUTHOR INFORMATION

### Corresponding Author

\*E-mail: v.barone@cmich.edu.

### Present Addresses

<sup>§</sup>Current address: Centro de Investigacion en Materiales Avanzados, SC Unidad Monterrey, Alianza Nte. 202, Apodaca, NL Mexico, CP 66600, Mexico.

### Notes

The authors declare no competing financial interest.

## ACKNOWLEDGMENTS

V.B. acknowledges the donors of The American Chemical Society Petroleum Research Fund for support of this research through the award ACS PRF #49427-UNI6. A.H.R. thanks the support of Conacyt-Mexico under projects 152153 and TAMU-CONACyT binational collaboration. We also recognize the computational time provided by the CNS-IPICyT, Mexico and the Texas Supercomputer Center, TACC.

## REFERENCES

- (1) Novoselov, K. S.; Geim, A. K.; Morozov, S. V.; Jiang, D.; Zhang, Y.; Dubonos, S. V.; Grigorieva, I. V.; Firsov, A. A. *Science* **2004**, *306*, 666–669.
- (2) Nakada, K.; Fujita, M.; Dresselhaus, G.; Dresselhaus, M. S. *Phys. Rev. B* **1996**, *54*, 17954–17961.
- (3) Berger, C.; Song, Z.; Li, X.; Wu, X.; Brown, N.; Naud, C.; Mayou, D.; Li, T.; Hass, J.; Marchenkov, A. N.; Conrad, E. H.; First, P. N.; de Heer, W. A. *Science* **2006**, *312*, 1191–1196.
- (4) Son, Y.-W.; Cohen, M. L.; Louie, S. G. *Nature* **2006**, *444*, 347–349.
- (5) Son, Y.-W.; Cohen, M. L.; Louie, S. G. *Phys. Rev. Lett.* **2006**, *97*, 216803.
- (6) Ezawa, M. *Phys. Rev. B* **2006**, *73*, 045432.
- (7) Barone, V.; Hod, O.; Scuseria, G. E. *Nano Lett.* **2006**, *6*, 2748–2754.
- (8) Han, M. Y.; Oezilmaz, B.; Zhang, Y.; Kim, P. *Phys. Rev. Lett.* **2007**, *98*, 206805.
- (9) Chen, Z.; Lin, Y.-M.; Rooks, M. J.; Avouris, P. *Physica E* **2007**, *40*, 228–232.
- (10) Krepel, D.; Hod, O. *Surf. Sci.* **2011**, *605*, 1633–1642.
- (11) Kan, E. J.; Li, Z.; Yang, J.; Hou, J. G. *Appl. Phys. Lett.* **2007**, *91*, 243116.
- (12) Hod, O.; Barone, V.; Peralta, J. E.; Scuseria, G. E. *Nano Lett.* **2007**, *7*, 2295–2299.
- (13) Wang, X.; Ouyang, Y.; Li, X.; Wang, H.; Guo, J.; Dai, H. *Phys. Rev. Lett.* **2008**, *100*, 206803.
- (14) Yang, X.; Dou, X.; Rouhanipour, A.; Zhi, L.; Rader, H. J.; Mullen, K. *J. Am. Chem. Soc.* **2008**, *130*, 4216–4217.
- (15) Kosynkin, D. V.; Higginbotham, A. L.; Sinitskii, A.; Lomeda, J. R.; Dimiev, A.; Price, B. K.; Tour, J. M. *Nature* **2009**, *458*, 872–US.
- (16) Jiao, L.; Zhang, L.; Wang, X.; Diankov, G.; Dai, H. *Nature* **2009**, *458*, 877–880.
- (17) Cervantes-Sodi, F.; Csányi, G.; Piscanec, S.; Ferrari, A. C. *Phys. Rev. B* **2008**, *77*, 165427.
- (18) Khantha, M.; Cordero, N. A.; Molina, L. M.; Alonso, J. A.; Girifalco, L. A. *Phys. Rev. B* **2004**, *70*, 125422.
- (19) Valencia, F.; Romero, A.; Ancilotto, F.; Silvestrelli, P. *J. Phys. Chem. B* **2006**, *110*, 14832–14841.
- (20) Chan, K.; Neaton, J.; Cohen, M. *Phys. Rev. B* **2008**, *77*, 235430.
- (21) Rigo, V. A.; Martins, T. B.; da Silva, A. J. R.; Fazzio, A.; Miwa, R. H. *Phys. Rev. B* **2009**, *79*, 075435.
- (22) Ataca, C.; Akturk, E.; Ciraci, S.; Ustun, H. *Appl. Phys. Lett.* **2008**, *93*, 043123.
- (23) Sevincli, H.; Topsakal, M.; Durgun, E.; Ciraci, S. *Phys. Rev. B* **2008**, *77*, 195434.
- (24) Choi, S.-M.; Jhi, S.-H. *Phys. Rev. Lett.* **2008**, *101*, 266105.
- (25) Schlapbach, L.; Zuttel, A. *Nature* **2001**, *414*, 353–368.
- (26) Winter, M.; Besenhard, J.; Spahr, M.; Novák, P. *Adv. Mater.* **1998**, *10*, 725–763.
- (27) Kaskhedikar, N.; Maier, J. *Adv. Mater.* **2009**, *21*, 2664–2680.
- (28) Profeta, G.; Calandra, M.; Mauri, F. *Nature Phys.* **2012** [Online].
- (29) Yoo, E.; Kim, J.; Hosono, E.; Zhou, H.; Kudo, T.; Honma, I. *Nano Lett.* **2008**, *8*, 2277–2282.
- (30) Deng, W.-Q.; Xu, X.; Goddard, W. *Phys. Rev. Lett.* **2004**, *92*, 166103.
- (31) Sun, Q.; Jena, P.; Wang, Q.; Marquez, M. *J. Am. Chem. Soc.* **2006**, *128*, 9741–9745.
- (32) Mpourmpakis, G.; Tylianakis, E.; Froudakis, G. *Nano Lett.* **2007**, *7*, 1893.
- (33) Baker, T. A.; Head-Gordon, M. *J. Phys. Chem. A* **2010**, *114*, 10326–10333.
- (34) Jin, K.-H.; Choi, S.-M.; Jhi, S.-H. *Phys. Rev. B* **2010**, *82*, 033414.
- (35) Rabii, S.; Guerard, D. *J. Phys. Chem. Sol.* **2008**, *69*, 1165–1167.
- (36) Mapasha, R.; Chetty, N. *Comput. Mater. Sci.* **2010**, *49*, 787–791.
- (37) Kresse, G.; Furthmüller, J. *Phys. Rev. B* **1996**, *54*, 11169–11186.
- (38) Kresse, G.; Furthmüller, J. *Comput. Mater. Sci.* **1996**, *6*, 15–50.
- (39) Perdew, J. P.; Burke, K.; Ernzerhof, M. *Phys. Rev. Lett.* **1997**, *78*, 1396.
- (40) Blöchl, P. E. *Phys. Rev. B* **1994**, *50*, 17953–17979.
- (41) Uthaisar, C.; Barone, V. *Nano Lett.* **2010**, *10*, 2838–2842.
- (42) Uthaisar, C.; Barone, V.; Peralta, J. E. *J. Appl. Phys.* **2009**, *106*, 113715.
- (43) Medvedev, N. *J. Comp. Phys.* **1986**, *67*, 223–229.
- (44) Frank, I. W.; Tanenbaum, D. M.; Van der Zande, A. M.; McEuen, P. L. *J. Vac. Sci. Technol. B* **2007**, *25*, 2558–2561.
- (45) Meyer, J. C.; Geim, A. K.; Katsnelson, M. I.; Novoselov, K. S.; Booth, T. J.; Roth, S. *Nature* **2006**, *446*, 60–63.
- (46) Xiao, X.; Liu, P.; Wang, J. S.; Verbrugge, M.; Balogh, M. P. *Electrochim. Commun.* **2010**, *13*, 209–212.
- (47) Yang, C.-K. *Appl. Phys. Lett.* **2009**, *94*, 163115.